Food & Function

ROYAL SOCIETY OF CHEMISTRY

PAPER

View Article Online
View Journal | View Issue



Cite this: *Food Funct.*, 2023, **14**, 3712

# Structural characterization of a sulfated polysaccharide from *Gracilariopsis lemaneiformis* and its potentiation of cisplatin antitumor activity in Colon-26 carcinoma tumor-bearing mice by inducing ferroptosis

Bingna Cai,[a,b] Lianxiang Luo,[c] Xiaodan Chen,[d] Xiangtan Zhao,[a] Jiake He,[c] Hua Chen,[a,b] Peng Wan,[a,b] Deke Chen[a] and Jianyu Pan *[a,b]

Ferroptosis, a form of regulated cell death caused by iron-mediated lipid peroxidation, has become a potential strategy to overcome drug resistance and improve the efficacy of traditional cancer treatments. In this study, we investigated whether treatment with the combination of *Gracilariopsis lemaneiformis* polysaccharides and cisplatin (CP) potentiated the antitumor activity in a Colon-26 carcinoma tumor-bearing mouse model by ferroptosis activation. The *G. lemaneiformis* polysaccharide GP90 was mainly composed of (1→3) linked 4-*O*-sulfate-β-D-galactose and (1→4) linked 3,6-anhydro-α-L-galactose with a molecular weight of 12.45 kDa. Compared with the CP group, the combination of GP90 and CP significantly suppressed tumor growth. Based on the transcriptomic and metabolomic analyses of tumor tissue, GP90 enhanced the antitumor effect of CP by promoting ferroptosis and regulating ferroptosis-related metabolic pathways. Moreover, the accumulation of 4-hydroxy-2-nonenal (4-HNE) and down-regulation of the expression of solute carrier family 7 member 11 (SLC7A11) and glutathione peroxidase 4 (Gpx4) were verified by immunohistochemistry staining. Finally, gene set enrichment analysis showed that positive immunoregulatory pathways were significantly enriched in the GP90 and CP combination group. Our results indicate that GP90 potentiates chemotherapy sensitivity by targeting the transferrin receptor and SLC7A11/Gpx4 pathway to induce ferroptosis, which might be a useful therapeutic target in colorectal cancer patients.

Received 1st January 2023,
Accepted 17th March 2023

DOI: 10.1039/d3fo00009e

rsc.li/food-function



## 1. Introduction

Colorectal cancer (CRC) is the third most common malignancy and the second leading cause of cancer-related death,[1] with nearly 1.93 million new cases and 0.94 million deaths in 2020 worldwide.[2] Cisplatin (CP) is one of the most effective cytotoxic agents in CRC chemotherapy; however, its therapeutic efficacy is limited by chemoresistance and detrimental side effects.[3] Hence, there remains a need for effective therapeutic approaches to improve the CP sensitivity in CRC. Recent scientific evidence has shown that CP induces ferroptosis and apoptosis in CRC cells and that the combination of CP and the ferroptosis inducer erastin is effective in enhancing the antitumor activity of drugs.[4] Ferroptosis, a new mode of cell death caused by iron-dependence and lipid peroxidation, plays a beneficial role in improving cancer treatment, tumor chemoresistance, and antitumor immunotherapy. Ferroptosis agonists can promote the accumulation of intracellular reactive oxygen species (ROS), reduce the transferrin content, or inhibit cystine/glutamate antiporter System Xc-mediated cystine transport, which leads to ferroptosis in drug-resistant tumor cells.[5] In addition, ferroptosis may reshape the tumor ecology and stimulate the immune microenvironment, thereby inhibiting tumor growth and progression.[6] Thus, strategies to induce ferroptosis have been proposed to improve the outcomes of current cancer therapy.

*Gracilariopsis lemaneiformis* is an edible red alga of economic importance that is not only directly consumed but can also be processed into dietary supplements, cosmetics, and

[a]*Key Laboratory of Tropical Marine Bio-resources and Ecology, Guangdong Key Laboratory of Marine Materia Medica, South China Sea Institute of Oceanology, Chinese Academy of Sciences, 164 West Xingang Road, Guangzhou 510301, Guangdong, China. E-mail: jypan@scsio.ac.cn; Fax: +86 20 84451515; Tel: +86 20 89023145*
[b]*Innovation Academy of South China Sea Ecology and Environmental Engineering (ISEE), Chinese Academy of Sciences, Guangzhou 510000, China*
[c]*Experimental Animal Center, Guangdong Medicial University, Zhanjiang 524023, Guangdong, China*
[d]*Guangdong Provincial Key Laboratory of Food Quality and Safety, College of Food Science, South China Agricultural University, Guangzhou 510642, China*

pharmaceuticals, among others. *G. lemaneiformis* contains high levels of polysaccharides, phycobiliproteins, pigments, and other nutritional components, whereas polysaccharides are its main active components.[7] *G. lemaneiformis* polysaccharides (GPs) exert potential antitumor activity without obvious toxicity. Shi *et al.* reported that the three polysaccharides extracted from *G. lemaneiformis* inhibited the proliferation of MCF-7, HepG-2, and HeLa cells *in vitro*.[8] Additionally, *in vivo* antitumor tests showed that soluble GPs significantly inhibited mouse sarcoma S180 tumor growth and improved the activity of splenic lymphocytes and natural killer cells.[9] Moreover, GPs alleviated dextran sulfate sodium-induced colitis in mice by remodelling the gut microbiota and intestinal metabolites, which reduces the risk of CRC.[10] Thus, GPs not only directly inhibit tumor growth, but also interfere with tumor progression and can be used for tumor prevention and adjuvant therapy. Du *et al.* found that *Lycium barbarum* polysaccharide effectively prevented the proliferation and promoted the ferroptosis of breast cancer cells, mainly by the System Xc- and glutathione peroxidase 4 (Gpx4) pathway.[11] Studies have also shown that *Pinus massoniana* pollen polysaccharide treated colon cells exhibit electron-lucent cytoplasm and nuclei as well as cytoplasmic vacuolization, which are characteristic of apoptosis caused by ferroptosis.[12] The question remains whether the auxiliary antitumor activity of GPs is related to the induction of ferroptosis.

In this study, we investigated the synergistic antitumor effect of GPs in combination with CP and determined whether the underlying mechanism is related to ferroptosis induction.

## 2. Materials and methods

### 2.1. Materials

Dried *G. lemaneiformis* was provided by Qingdao Haiyouyou Trading Co., Ltd (Shandong, China), the origin being Qingdao. Colon-26 (C26) colon carcinoma cell lines were obtained from the American Type Culture Collection (ATCC, Manassas, VA, USA). Dulbecco's modified Eagle medium (DMEM), fetal bovine serum (FBS), penicillin–streptomycin antibiotics, and phosphate-buffered saline (PBS) were purchased from Invitrogen-Gibco (Grand Island, NY, USA). All chemical reagents were of analytical grade.

### 2.2. Preparation of GP90

Dried *G. lemaneiformis* powder was obtained by crushing and passing through an 80-mesh screen. Then the powder was washed three times with anhydrous ethanol, and soaked overnight in anhydrous ethanol at 4 °C. After filtration, the filtered residue was dried at 70 °C for 2 h and then extracted with 35 times the volume of 0.05 M citric acid solution (v/w, mL $g^{-1}$) at 100 °C. After the reaction for 2 h, the supernatant was collected by centrifugation at 10 000 rpm for 20 min, and the pH was adjusted to 7.0 with 1 M NaOH solution and concentrated. The concentrate was recovered, and anhydrous ethanol was added until the concentration of the final system alcohol was 30% for precipitating the fraction, followed by a continued regulation of the supernatant with anhydrous ethanol to final alcohol concentrations of 60% and 90% to obtain GP90. The precipitated GP90 was solubilized with distilled water, deproteinated by the Sevag method (chloroform : butanol = 5 : 1, v/v), concentrated, dialyzed, and lyophilized.

### 2.3. Structural characterization of GP90

The homogeneity and molecular weight were measured with an Agilent 1260 Infinity size exclusion chromatography and gel permeation chromatography system equipped with an Agilent RID-7115A refractive index detector (Agilent Technologies, Palo Alto, CA, USA) and a gel-filtration chromatography column (TSK-gel G3000PWXL column, 7.8 × 300 mm i.d., 7 μm; Tosoh Bioscience LLC, Tokyo, Japan). Dextran standards (1, 5, 12, 50, 80 and 270 kDa) were used for calibration. Elution was performed with 0.02 M ammonium acetate solution at a rate of 0.6 mL $min^{-1}$ and maintained at 35 ± 1 °C.

According to a previously reported high-performance liquid chromatography (HPLC) method,[13] freeze-dried GP90 (5 mg) was hydrolysated with 4 M trifluoroacetate acid (TFA, 1 mL) for 4 h at 120 °C, and excess TFA was removed by rotary evaporation with methanol. Subsequently, the products or monosaccharide standards were derivatized with 3-methyl-1-phenyl-2-pyrazolin-5-one (PMP, 0.5 M) at 70 °C for 1.5 h. Then the reaction mixture was neutralized and excess PMP was removed using chloroform. The monosaccharide was analyzed using HPLC (Agilent-1260; Agilent Technologies) equipped with a YMC-Pack ODS-AQ column (250 × 4.6 mm, I.D. S-5 μm, 12 nm) and eluted with 50 mM ammonium acetate solution and acetonitrile at a ratio of 73 : 17 (v/v).

Fourier transform infrared spectroscopy (FTIR) for GP90 was carried out using 400 FT-IR spectrometers (Shimadzu, Japan) at wavelengths ranging from 4000 to 400 $cm^{-1}$.

GP was prepared with $D_2O$ to a concentration of 30 mg $mL^{-1}$. The nuclear magnetic resonance (NMR) spectra of GP90 were analyzed using a 700 MHz NMR spectrometer (Bruker Daltonik GmbH, Leipzig, Germany), and the 1D- and 2D-NMR spectra were recorded.

### 2.4. Animal experimental design

BALB/c mice (8 weeks old, 20–24 g, male) were obtained from SiPeiFu (Beijing Biotechnology Co., Ltd, Beijing, China) and housed in a room under a 12 h light–dark cycle and maintained at 22 ± 2 °C. Animal experiments were performed following the guidelines of the Animal Ethics Committee of Guangdong Medical University (GDY1902062).

C26 colorectal models were prepared as described by Zhang *et al.*[14] Briefly, C26 colon cells were cultured in DMEM containing 10% FBS, 1% glutamine, 1 mM sodium pyruvate, and 1% streptomycin/penicillin at 37 °C and 5% $CO_2$. Then the cells were collected in a 0.25% trypsin-EDTA solution and resuspended in sterile PBS before subcutaneous injection into mice ($1 \times 10^6$ cells per mouse). On day 1 after the C26 cell injection, all mice were randomly divided into four groups: model, GP90, CP and CP + GP90.[15] Mice in the GP90 and CP + GP90 groups

were gavaged with 200 mg $kg^{-1}$ GP90 daily, whereas mice in the other two groups were gavaged with 0.2 mL sterile saline alone daily. In CP and CP + GP90 groups, the mice were treated with a combination of GP90 and intraperitoneal CP chemotherapy (3 mg $kg^{-1}$) starting from day 1 and every 4 days thereafter. During the study, the tumor volume was measured every 3 days based on the formula: $V = 0.5x^2y$, where $x$ is the shortest and $y$ is the largest superficial diameter. On day 16 after treatment, the mice in all groups were sacrificed by cervical dislocation. Spleen and tumor tissues were collected and stored at −80 °C for subsequent analyses.

### 2.5. RNA isolation, sequencing, and bioinformatics analysis

Total RNA from tumor samples was extracted using the Trizol reagent (Invitrogen, Carlsbad, CA, USA) based on the manufacturer's protocol, and the RNA quality was assessed using RNase-free agarose gel electrophoresis using an Agilent 2100 Bioanalyzer (Agilent Technologies). After the extraction of total RNA, eukaryotic mRNA was enriched using oligo (dT) beads, while rRNA was removed using the Ribo-ZeroTM Magnetic Kit (Epicentre, Madison, WI, USA). Then the enriched mRNA was fragmented into short fragments with fragmentation buffer and reverse transcribed into cDNA using random primers. The cDNA fragments were purified using the QiaQuick PCR extraction Kit (Qiagen, Venlo, the Netherlands), end-repaired, polyadenylated, and ligated to Illumina sequencing adapters. The ligation products were separated by size by agarose gel electrophoresis, amplified by PCR, and sequenced using the Illumina HiSeq2500 (Gene Denovo Biotechnology Co., Guangzhou, China). The RNA-sequence data reported in this study was archived in the NCBI SRA database with the accession number PRJNA945228 and PRJNA945586.

The differential expression analysis of different RNAs in each group was performed using the DESeq2 software. The genes with a false discovery rate parameter below 0.05 and an absolute fold change ≥2 were considered differentially expressed genes (DEGs). All DEGs were mapped to Gene Ontology (GO) terms in the GO database (**https://www.geneontology.org/**), and then the number of genes per term was calculated. The GO terms that were significantly enriched in DEGs were defined using the hypergeometric test. The Kyoto Encyclopedia of Genes and Genomes (KEGG) pathway enrichment analysis identified metabolic pathways or signal transduction pathways that were significantly enriched in DEGs compared to the genome-wide background. The calculated $p$-value was corrected for the false discovery rate (FDR) with an FDR of ≤0.05 as the threshold. GO terms and KEGG pathways that met this condition were defined as significantly enriched in DEGs.

### 2.6. Metabolite analysis

Tumor tissues (100 mg) were grounded with liquid nitrogen and resuspended in 500 μL prechilled 80% methanol by vortexing. The homogenate was incubated on ice for 5 min and then centrifuged at 15 000$g$, 4 °C for 20 min. The supernatant was taken and diluted with LC-mass spectrometry (MS) grade water to a final methanol concentration of 53%, and then centrifuged at 15 000$g$, 4 °C for 20 min. Finally, the supernatant was injected into an LC-tandem MS (MS/MS) system for analysis.

Ultra-performance LC (UPLC)-MS/MS analysis was performed using the Vanquish UPLC system (Thermo Fisher Scientific, Dreieich, Germany) coupled with the Orbitrap Q ExactiveTM HF-X mass spectrometer (Thermo Fisher Scientific) at Gene Denovo Co., Ltd. Samples were injected into a Hypesil gold column (100 × 2.1 mm, 1.9 μm) at a flow rate of 0.2 mL $min^{-1}$. The eluents for the positive polarity mode were eluent A (0.1% formic acid in water) and eluent B (methanol), and the eluents for the negative polarity mode were eluent A (5 mM ammonium acetate, pH 9.0) and eluent B (methanol). The elution parameters were set as follows: 2% B, 1.5 min; 2–100% B, 12.0 min; 100% B, 14.0 min; 100–2% B, 14.1 min; and 2% B, 17.0 min. A Q Exactive™ HF-X mass spectrometer was operated using a spray voltage of 3.2 kV, a capillary temperature of 320 °C, a sheath gas flow rate of 40 arb, and an aux gas flow rate of 10 arb.

Raw data files generated by UPLC-MS/MS were processed using the Compound Discoverer 3.1 (Thermo Fisher Scientific) for peak alignment, peak extraction, and quantitation for each metabolite. Then peak intensities were normalized to the total spectral intensity and matched against mzCloud (**https://www.mzclound.org/**), mz Vault, and the Mass List database to obtain accurate qualitative and relative quantitative results. Statistical analyses were performed using Python (Python 2.7.6 version), R (R version R-3.4.3), and the CentOS (CentOS release 6.6) statistical software.

Orthogonal projections to latent structure-discriminant analysis (OPLS-DA) were performed in metaX. Metabolites with variable importance in projection values >1 and a $p$-value of the $t$-test <0.05 were considered to be differentially expressed metabolites (DEMs). The functions of DEMs and metabolic pathways were analyzed using the KEGG database. The $P$-Value <0.05 was considered statistically significant.

### 2.7. Quantitative PCR

The gene expression was validated based on the transcriptomic data using quantitative PCR (qPCR). Total RNA was prepared using the Trizol reagent. HiScript II Q RT SuperMix was used for the qPCR of complementary DNA. Quantitative PCR was performed with the AceQ qPCR SYBR Green Master Mix (Vazyme, Nanjing, China) on the TL988 device (TianLong Group, Guangdong, China). The amplifying conditions for cDNA were as follows: denaturation at 95 °C for 90 s, 40 cycles of 95 °C for 5 s, and 60 °C for 15 s, followed by 72 °C for 20 s. The $2^{-\Delta\Delta Ct}$ method was applied to calculate changes in the mRNA expression levels of candidate genes. The primer sequences are listed in Table 1.

### 2.8. Immunohistochemistry staining

Tumor tissues were weighed, fixed in 10% formalin, and embedded in paraffin. Briefly, after deparaffinization and blocking in 3% hydrogen peroxide, the sections were treated with citric sodium buffer (1 M, pH 6.0) and then treated by

Table 1 Sequences of qPCR primers

| Gene | Forward sequence | Reverse sequence |
|---|---|---|
| Apoe | CTGAACCGCTTCTGGGATTA | GTTGCGTAGATCCTCCATGT |
| Tfrc | CAGTCATCAGGGTTGCCTAATA | CTGGGCTCCTACTACAACATAAC |
| Bnip3 | TCCAGCCTCCGTCTCTATTT | CGACTTGACCAATCCCATATCC |
| β-Actin | CTGAGTCTCCCTTGGATCTTTG | AGGGCAGGTGAAACTGTATG |

microwave for antigen unmasking. Sections were blocked and then incubated with anti-4-hydroxy-2-nonenal (4-HNE, 1 : 1600 dilution; Bioss Antibodies, Massachusetts, USA), anti-solute carrier family 7 member 11 (SLC7A11, 1 : 1600 dilution; Cell Signaling Technology [CST], Shanghai, China), and anti-GPX4 (1 : 1600 dilution; CST) primary antibodies at 4 °C overnight. The next day, sections were incubated with horseradish peroxidase labelled secondary antibody (1 : 5000 dilution; CST) for 1 h at room temperature and then rinsed three times with PBS. The sections were coloured with DAB, counterstained with hematoxylin, and dehydrated. All images were viewed using the FilterMax F5 fluorescence microplate reader (Molecular Devices, Silicon Valley, CA, USA).

### 2.9. Statistical analyses

All data are expressed as the mean ± standard deviation (SD). Differences were analyzed by the one-way analysis of variance using the IBM SPSS 22.0 software. $P < 0.05$ was considered statistically significant.

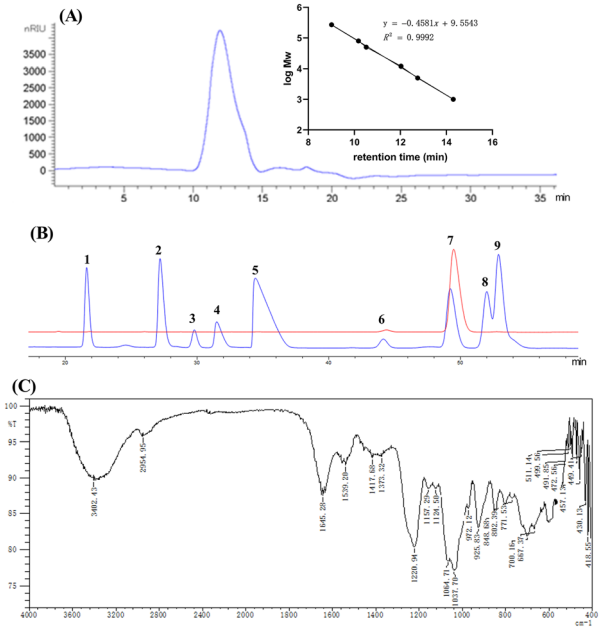


Fig. 1 Molecular weight distribution (A), monosaccharide composition (B), and FT-IR spectra of GP90 (C). The HPLC chromatograms of monosaccharide standards (blue line) and GP90 (red line). Peaks 1 = Man, 2 = Rib, 3 = Rha, 4 = GlcA, 5 = GalA, 6 = Glc, 7 = Gal, 8 = Xyl and 9 = Ara.

## 3. Results

### 3.1. Structural characterization of GP90

The contents of carbohydrates and sulfate in GP90 were 88.29 ± 8.24% and 22.93 ± 0.94%, respectively. A single and sharp peak was observed in the chromatogram of GP90 (Fig. 1A) with an average molecular weight of 12.45 kDa. GP90 was mainly composed of galactose (97.95%; Fig. 1B), which indicated that GP90 was a homogeneous polysaccharide. As shown in Fig. 1C, the FTIR spectrum of GP90 showed typical characteristic peaks of polysaccharides. The broad absorption at 3402.43 $cm^{-1}$ and sharp absorption at 2954.95 $cm^{-1}$ were O–H and C–H stretching vibrations, respectively. The strong absorption peak at 1220.94 $cm^{-1}$ and the sharp absorption peak at 848.68 $cm^{-1}$ corresponded to the asymmetric stretching vibrations of S=O and C–O–S, respectively, which indicates the presence of sulfate.[16] Peaks between 1000 and 1200 $cm^{-1}$ may have the presence of C–O–H and C–O–C of galactose.[17] The peaks at 925.83 and 848.68 $cm^{-1}$ indicated the presence of 3,6-anhydro-galactopyranose and axial sulfate ester at C4 of D-galactopyranose (G4S), respectively.[18] The low-intensity peak at 802.39 $cm^{-1}$ was thought to be the sulfate group at C-2 of 3,6-anhydro-galactopyranose.[19] The results revealed that GP90 was composed of galactose and anhydro-galactose.

The 1D NMR ($^1H$, $^{13}C$, and DEPT-135) and 2D NMR (heteronuclear singular quantum correlation spectroscopy [HSQC], heteronuclear multiple correlation spectroscopy [HMBC], and correlation spectroscopy [COSY]) were performed to analyze the structural configurations of GP90. As shown in the $^1H$ NMR spectrum of GP90 (Fig. 2A), a typical proton of the anomeric carbon of 3,6-anhydrogalactose (DA) at $\delta$ 5.02 and of galactose-4-sulfate (G4S) at $\delta$ 4.54 are characteristic of κ-carrageenan.[17,19] The ratio of G4S/DA was 2.34, which was calculated based on the H-4 proton of G4S and the H-1 signal of DA.[20] The signals at $\delta$ 102.27 and $\delta$ 94.34 (Fig. 2B) were ascribed to C-1 of G4S and DA, respectively.[21] From the DEPT-135 spectrum (Fig. 2C), the intense inverted peak at $\delta$ 60.73 was the C-6 of D4S, whereas the other inverted peak at $\delta$ 69.40 was the C-6 of DA. The assignment of GP90 was analyzed with 2D NMR. The $^1H$ and $^{13}C$ chemical shifts of GP90 are summarized in Table 2. The HSQC spectrum depicts the correlations of anomeric carbons of G4S with protons at $\delta$ 102.27/4.54 and $\delta$ 94.34/5.02 for DA (Fig. 2D). From the COSY spectrum of GP90 (Fig. 2E), the coupling correlation between H-1 ($\delta$ 4.54) and H-2 ($\delta$ 3.42), H-3 ($\delta$ 3.73) and H-4 ($\delta$ 4.59), and H-5 ($\delta$ 3.72) and H-6 ($\delta$ 3.71) of G4S were found. For DA, H-1/H-2 was at $\delta$ 5.02/4.05, H-2/H-3 was at $\delta$ 4.05/4.43, and H-5/H-6 was

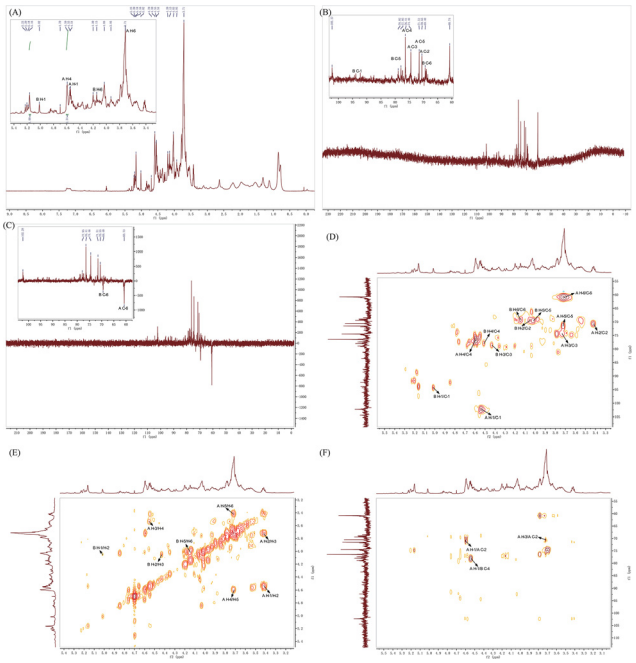

Fig. 2 The structural characterization of GP90 (A) $^{1}$H NMR spectrum, (B) $^{13}$C NMR spectrum, (C) DEPT135 spectrum, (D) HSQC spectrum, (E) COSY spectrum and (F) HMBC spectrum. DEPT: distortionless enhancement by polarization transfer; COSY: homonuclear chemical shift correlation spectroscopy; HSQC: heteronuclear singular quantum correlation spectroscopy; and HMBC: heteronuclear multiple correlation spectroscopy.

Table 2 $^{1}$H and $^{13}$C NMR chemical shifts of GP90

| Sugar residues | $^{1}$H/$^{13}$C chemical shift (ppm) | | | | | |
|---|---|---|---|---|---|---|
| A (1→3) linked 4-*O*-sulfate-β-D-galactose | 4.54 | 3.42 | 3.73 | 4.59 | 3.72 | 3.71 |
| | 102.27 | 70.55 | 74.45 | 76.41 | 71.51 | 60.73 |
| B (1→4) linked 3,6-anhydro-α-L-galactose | 5.02 | 4.05 | 4.43 | 4.51 | 4.02 | 4.15 |
| | 94.34 | 69.54 | 78.67 | 77.97 | 69.54 | 69.40 |

at 4.02/4.15. The linkage sites of G4S and DA in GP90 were further confirmed from the HMBC NMR spectrum shown in Fig. 2F. The cross-peak at $\delta$ 4.54/77.91 (A H-1/B C-4) revealed that the O-1 of residue A was linked to the C-4 of residue B. The results of NMR spectroscopy also confirmed the presence of (1→3) linked 4-*O*-sulfate-β-D-galactose and (1→4) linked 3,6-anhydro-α-L-galactose. This similar structure of sulfated galactans has been found in other red algae such as *Gracilari caudate*, *Gracilariopsis persica*, *Ahnfeltiopsis flabelliformis*, and *Acanthophora spicifera*.[22–25]

### 3.2. The antitumor effect of GP90

The C26 tumor-bearing mice were treated with GP90 for 15 days and were sacrificed on day 16. Compared with the model group, tumor growth was significantly inhibited in GP90-treated mice starting from day 10 after the tumor challenge (Fig. 3A). The average tumor weight in the GP90 group was decreased by 24.01% compared to that in the model group

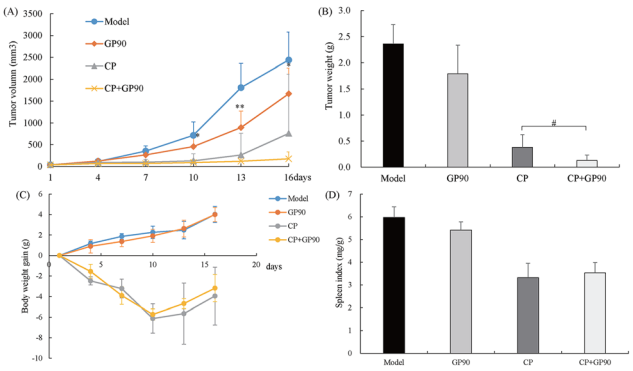


Fig. 3 GP90 exerted antitumor efficacy in the C26 carcinoma tumor-bearing mice. (A) The tumor growth curve was reported using the tumor volume one time per 3 days. (B) The average tumor weight for each group on the last day (*i.e.*, day 16). (C) The average weight gain of mice every three days. Results are expressed as the mean ± SD ($n$ = 6). *$p$ < 0.05, **$p$ < 0.01, the model group *vs*. the GP90 group; #$p$ < 0.05, the CP group *vs*. the CP + GP90 group.

(Fig. 3B). In addition, the tumor growth of CP-treated mice was obviously inhibited, and the tumor inhibition rate was significantly increased to 94.55% when combined with GP90 (Fig. 3B). During the experiment, GP90 treatment had no significant effect on the mouse body weight and spleen index (Fig. 3C and 3D), suggesting that GP90 inhibited tumor growth without exerting general toxicity to the host. These results indicate that GP90 exerts potential antitumor effects and increases the sensitivity of tumor cells to CP.

### 3.3. Antitumor effect of the GP90 and CP combination treatment is associated with ferroptosis

To elucidate the potential mechanism of the combined antitumor activity of GP90 and CP, the transcriptome and metabolome were used to analyze the changes in the tumor tissue. A total of 22 322 genes were annotated in the tumor tissue from the CP + GP90 group, of which there were 13 DEGs (five upregulated and eight downregulated) compared with the CP group (Fig. 4A). GO enrichment results showed that the DEGs were significantly enriched in biological processes such as localization, immune system response, and signalling; molecular functions such as binding, catalytic activity, and transporter activity; and significant enrichment in cellular components such as membrane, protein-containing complexes and the extracellular region (Fig. 4B). KEGG pathway terms enriched by DEGs were mainly involved in nitrogen metabolism, ferroptosis, and cholesterol metabolism (Fig. 4C). qPCR analysis of ferroptosis-related genes apolipoprotein (Apoe), transferrin receptor (Tfrc) and B-cell lymphoma 2-interacting protein 3 (Bnip3) in tumor tissues was performed to validate the RNA-seq results. Compared with the CP group, the relative mRNA expression of Apoe and Tfrc was up-regulated, whereas the relative mRNA expression of Bnip3 was down-regulated in the CP + GP90 group (Fig. 4D). Considering the DEGs and KEGG pathways involved in ferroptosis, we speculated that GP90

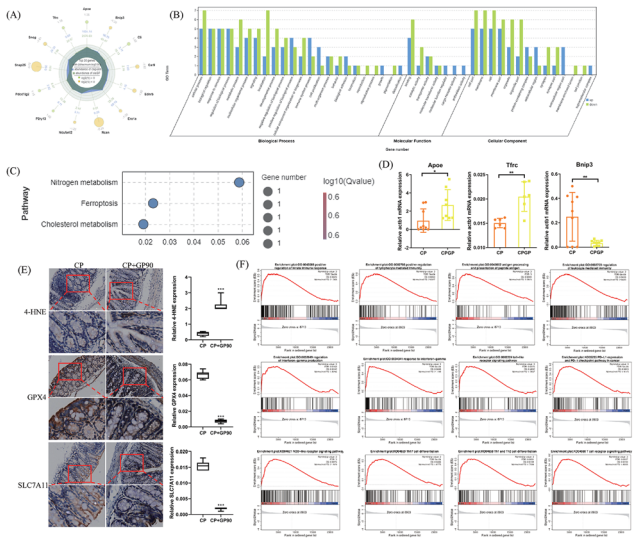

**Fig. 4** Transcriptomic analysis of the effect of GP90 on enhancing the CP sensitivity in the colon cancer tissue. (A) The radar chart of DEGs in CP *vs.* the CP + GP90 group. (B) Gene ontology analysis. (C) The most enriched KEGG pathways. (D) Quantification of ferroptosis-related genes by qPCR in the tumor tissue. (E) Immunohistochemistry staining for 4-HNE, SLC7A11, and Gpx4 in the tumor tissue. The original magnification of H & E is at 400×, and the width of the bar corresponds to 100 μm. (F) The gene set enrichment analysis (GSEA) of tumor tissue transcriptome data exhibited that C26 mice treated with the CP + GP90 combination therapy were significantly enriched in immune-related signalling pathways compared to mice treated with CP. The data are shown from at least four independent experiments. Results were accepted at |NES| > 1, NOM $p < 0.05$, FDR $q < 0.25$. Data are expressed as the mean ± SD; $^{*}p < 0.05$, $^{**}p < 0.01$, and $^{***}p < 0.001$ compared with the CP group.

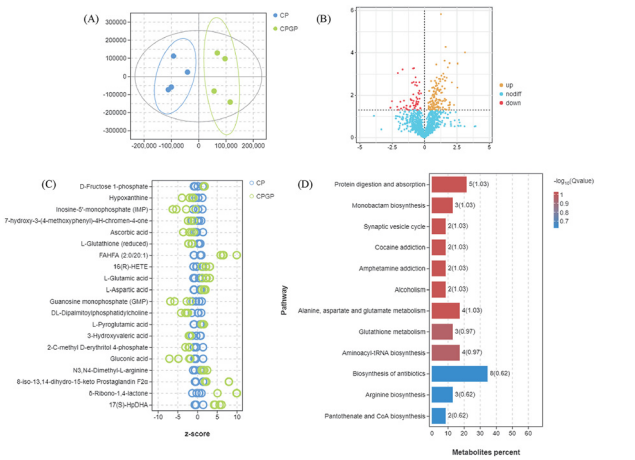

**Fig. 5** GP90 combined with cisplatin altered metabolic profiling in tumor tissue. (A) A volcano plot of differentially accumulated metabolites (DAMs), (B) the OPLS-DA score plot, (C) the Z-score plot of top 20 DAMs, and (D) the KEGG enrichment bar graph in the tumor tissue between the CP and CP + GP90 groups. Data are shown from four independent experiments.

could enhance the CP treatment sensitivity by inducing ferroptosis in tumor cells. The protein expression of ferroptosis-associated biomarkers including 4-HNE, Gpx4 and SLC7A11 in tumor tissues was identified by immunohistochemistry staining. Compared to the CP group, the relative expression of 4-HNE was clearly increased in the CP + GP90 group, whereas the relative expression of Gpx4 and SLC7A11 was sharply decreased (Fig. 4E). The gene set enrichment analysis (GSEA) results demonstrated various enriched immune- and tumor-related pathways in the GP + GP90 pathways, such as the positive regulation of the innate immune response, positive regulation of lymphocyte mediated immunity, antigen processing and presentation of peptide antigen, positive regulation of interferon-γ (IFN-γ) production, response to IFN-γ, Toll-like receptor signalling pathway, programmed death-ligand 1 (PD-L1) expression and programmed cell death protein 1 (PD-1) checkpoint pathway in cancer, nucleotide oligomerization domain (NOD)-like receptor signalling pathway, T helper 17 (Th17) cell differentiation, Th1 and Th2 cell differentiation and T cell receptor signalling (Fig. 4F).

The OPLS-DA plots for the CP and CP + GP90 groups show clustering in the respective regions (Fig. 5A). Compared with the CP group, there were 43 DAMs induced by the CP + GP90 group, and the volcano data show the distribution of the DEGs (Fig. 5B). Among the 43 DAMs, 27 genes were upregulated, and 16 genes were downregulated. These DAMs were mainly L-glutathione (reduced), L-glutamic acid, ascorbic acid, 17(*S*)-HpDHA, and 16(*R*)-HETE (Fig. 5C), which induced ferroptosis in tumor cells. The KEGG enrichment and pathway analysis showed that after GP90 treatment, the glutamate metabolism, glutathione metabolism, pantothenate and coenzyme A (CoA) biosynthesis were mainly regulated, which may be related to induced-ferroptosis of GP90 (Fig. 5D).

## 4. Discussion

CRC remains one of the most common malignancies worldwide. Among various chemotherapy drugs, CP is one of the most effective and widely used anticancer drugs for CRC. CRC initially responds to CP, followed by tumor recurrence after further treatment due to resistance, but does not affect CP-induced ferroptosis. Ferroptosis is a potentially novel strategy to address the problem of CP resistance. Studies have shown that CP combined with a ferroptosis inducer has a cumulative effect on its antitumor activity.[26] Polysaccharides have garnered great research interest in recent years because of their anticancer activity or can improve the efficacy of conventional chemotherapeutic drugs with fewer side effects.[27] The anticancer activity of some polysaccharides is related to the regulation of ferroptosis. Zhai *et al.* demonstrated that red ginseng polysaccharide induces ferroptosis effects on breast and lung cancer cells by targeting Gpx4.[28] Du *et al.* found that the anticancer activity of *L. barbarum* polysaccharide is related to the induction of ferroptosis in breast cancer cells.[11]

GPs induce transcriptional alternations and modulate lung cancer cell viability, morphology, and apoptosis.[29] In our study, it was found that GP90 can significantly decrease the

colon tumor volume after 13 days of the animal experiment. Previous studies have shown that the higher antitumor activities of polysaccharides may be related to their sulfate groups, which can selectively act as ligands on the cancer cell lines, forming molecular interactions that induce apoptosis.[30,31] GP90 has a relatively small molecular weight of 12.45 kDa and high sulfate content, accounting for 22.93%. It has been found that the polysaccharide activity increases with decreasing relative molecular weight in a certain molecular weight range.[7] A similar report showed that low molecular weight GPs (average molecular weight of 20.96 kDa) could effectively inhibit the growth of transplanted S180 tumors.[9] Smaller molecular GP fragments are tolerant to oral, gastric, and small intestinal conditions and reach the colon as a whole, are more easily metabolized by intestinal microbes, and have a better effect on cellular responses.[32]

GPs can significantly regulate the expression of apoptosis and cell cycle-related genes *via* the death receptor-mediated apoptosis pathway and the p53 pathway in A549 cell lines.[29] Fan *et al.* showed that acidic GPs significantly suppressed the proliferation of tumor in ICR mice transplanted with H22 hepatoma cells by increasing both specific and non-specific cellular immune responses.[33] In this study it has been found for the first time that GPs combined with CP could induce ferroptosis in the tumor tissue and sensitize the antitumor effect of CP in C26 tumor bearing-mice (Fig. 6). Transcriptomic results from tumor tissues showed that GP90 regulated the differential expression of genes related to ferroptosis in mice with CP chemotherapy. The combination treatment significantly increased the protein expression of Tfrc, which is a potential biomarker for colon adenocarcinoma initiation and progression and drug targets.[34] Dysregulated iron metabolism in CRC patients is highly correlated with their poor prognosis, and the iron transporter protein Tfrc mediates iron transport, promotes Tfrc mRNA stability, increases ROS production and iron death sensitivity, and enhances the host immune response to cancer.[35] In addition, Apoe expression associated with cholesterol metabolism is elevated, with similar results in adipocytes treated with ferric ammonium citrate resulting in an increased Apoe expression. Excess levels of cholesterol can also induce ferroptosis by elevating oxidative stress responses.[36] When cells become cancerous, the interaction between inflammation and tumors enhances ROS production, and the depletion of the mitotic receptor Bnip3, a key mitochondrial autophagy receptor in cells, promotes increased ROS levels and cell death.[37] Thus, Bnip3-depleted cells in GP90 combined with CP groups may contribute to tumor cell ferroptosis.

Based on these results, the ferroptosis-related proteins were validated, and an increase in the 4-HNE expression, and a decreased expression in Gpx4 and SLC7A11 were found in the CP + GP90 group. The final product of malondialdehyde, 4-HNE, produced by lipid peroxidation, may form covalent adducts with biomacromolecules, thereby reducing the membrane integrity and cross-linking, and inactivating proteins, and ultimately promoting cell membrane rupture and ferroptosis.[38] Recently, a growing number of studies have found that the induction of ferroptosis by increasing reactive oxygen species, decreasing intracellular levels of the antioxidant glutathione (GSH), or inactivating Gpx4 or SLC7A11 in CRC cells can facilitate the clinical treatment of CRC.[39] Gpx4, a key upstream regulator of ferroptosis, is the only glutathione peroxide used for intracellular lipid peroxidation reduction. If GSH is depleted or Gpx4 is inactivated, intracellular ferrous ions induce ferroptosis by breaking down phospholipid hydroperoxide leading to lipid peroxidation, which can be lethal to tumor cells.[40] Ferroptosis can be induced when lipid peroxide accumulates excessively, this process is tightly regulated by SLC7A11, known as System Xc-, a key component of the cysteine-glutamate antiporter.[41] Either knockdown of the SLC7A11 gene or inhibition of its activity increased ROS levels and decreased cysteine and glutathione levels, subsequently impairing the viability of colorectal cancer stem cells.[42] Thus, inhibition of the SLC7A11 expression usually leads to GSH depletion, which induces ferroptosis. These results are consistent with the decreased glutathione (reduced) and ascorbic acid and increased L-glutamic acid in the tumor tissue of GP90 combined with CP treatment. The KEGG enrichment analysis of the metabolomics of colon cancer tissues similarly showed that the combination of GP90 and CP affected the glutamate metabolism, glutathione metabolism, and pantothenate and CoA biosynthesis. Additionally, the related lipid metabolites such as 16(*R*)-HETE and 17(*S*)-HpDHA were increased. The increased DHA effectively activates ferroptosis-mediated tumor killing by promoting ROS accumulation, lipid peroxidation, and protein oxidation.[43] Inhibition of System Xc- has been reported to decrease the levels of CoA, which is synthesized from cysteine *via* the pantothenate pathway and plays a role in many metabolic pathways, particularly lipid metabolism, and can affect the sensitivity to ferroptosis.[44] This finding indicates that GP90 improves the CP treatment sensitivity by activating transferrin and reducing Gpx4- and SLC7A11-induced ferroptosis.

The onset of tumor ferroptosis and the resulting immune response trigger immunogenic cell death, as well as promote dendritic cell maturation and T cell infiltration. CD8+ T cells

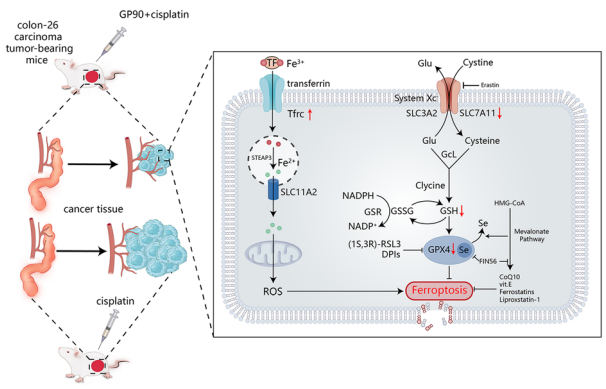


**Fig. 6** GP90 combined with cisplatin potentiates the antitumor activity *via* inducing ferroptosis targeting the Tfrc and SLC7A11/Gpx4 pathway.

can synergistically enhance T cell-regulated antitumor immune activity and promote the ferroptosis of tumor cells by downregulating IFN-γ release from SLC3A2 and SLC7A11, in conjunction with the immune checkpoint inhibitor PD-L1.[38] Therefore, from GSEA, GP90 combined with CP could positively regulate the innate immune response, promote the production and response of IFN-γ, and assist the immune checkpoint inhibitor PD-L1, which contribute to tumor cell death. Additionally, the Gpx4-deficient regulatory T cells elevate lipid peroxidation that facilitates Th17 responses and the promotion of antitumor immunity.[45] We have found that the combination of GP90 and CP promotes the Th17, Th1, and Th2 cell differentiation in response to the reduction in Gpx4. GP90 activated the innate immune response in combination with CP, and also involved the NOD-like receptor signalling pathway, Toll-like receptor signalling pathway, and T cell receptor signalling pathway, and plays a role in ferroptosis by regulating oxidative stress.[46] Further study will address the effect of GP90 on the immune function in CP-treated C26 carcinoma tumor-bearing mice.

## 5. Conclusions

In summary, we found that GP90 enhanced the antitumor effect of CP by promoting ferroptosis, which might be *via* targeting Tfrc and the SLC7A11/Gpx4 pathway. Furthermore, the combination treatment of GP90 and CP potentiated the cancer immunotherapy, which may be related to the NOD-like receptor, Toll-like receptor, T cell receptor, PD-L1 expression, and PD-1 checkpoint pathway. Overall, GP90 is a novel ferroptosis inducer and can be used as a functional food supplement for colon patients to promote chemotherapy sensitivity.

## Author contributions

The authors confirm the contribution to the paper as follows: Bingna Cai: conceptualization, data curation, formal analysis, writing – original draft preparation, funding acquisition, review and editing. Lianxiang Luo: methodology and validation. Xiaodan Chen: investigation and validation. Xiangtan Zhao: investigation and validation. Jiake He: visualization. Hua Chen: formal analysis and validation. Peng Wan: visualization and data curation. Deke Chen: data curation. Jianyu Pan: supervision, funding acquisition, review and editing. All authors have read and agreed to the published version of the manuscript.

## Conflicts of interest

There are no conflicts to declare.

## Acknowledgements

The authors are indebted to Dr Shikun Dai, Dr Zhihui Xiao, and Xiaohong Zheng (the Equipment Public Service Center, SCSIO, CAS) for their assistance with the high-speed refrigerated centrifuge and NMR spectrometric analysis. This work was supported by the National Natural Science Foundation of Guangdong, China (2022A1515010767), the Key-Area Research and Development Program of Guangdong Province (2020B1111030004), the Marine Economic Development Project (GDNRC[2023]38, GDNRC[2022]36), the Basic and Applied Basic Research Program of Guangdong Province (2019A1515110201), the Institution of South China Sea Ecology and Environmental Engineering, Chinese Academy of Sciences (ISEE2021PY05) and the Key Research and Development Program of Hainan Province (ZDYF2021SHFZ109).

## References

1 N. Keum and E. Giovannucci, Global burden of colorectal cancer: emerging trends, risk factors and prevention strategies, *Nat. Rev. Gastroenterol. Hepatol.*, 2019, **16**, 713–732, DOI: **10.1038/s41575-019-0189-8**.

2 Y. Xi and P. F. Xu, Global colorectal cancer burden in 2020 and projections to 2040, *Transl. Oncol.*, 2021, **14**, 101174, DOI: **10.1016/j.tranon.2021.101174**.

3 J. H. Yuan, X. M. Li, Y. Q. Zhang, G. Y. Zhang, W. P. Cheng, W. W. Wang, Y. B. Lei and G. Song, USP39 attenuates the antitumor activity of cisplatin on colon cancer cells dependent on p53, *Cell Biol. Toxicol.*, 2021, DOI: **10.1007/s10565-021-09683-0**.

4 J. Li, F. Cao, H. L. Yin, Z. J. Huang, Z. T. Lin, N. Mao, B. Sun and G. Wang, Ferroptosis: past, present and future, *Cell Death Dis.*, 2020, **11**, 88, DOI: **10.1038/s41419-020-2298-2**.

5 G. X. Xu, H. Wang, X. L. Li, R. M. Huang and L. X. Luo, Recent progress on targeting ferroptosis for cancer therapy, *Biochem. Pharmacol.*, 2021, **190**, 114584, DOI: **10.1016/j.bcp.2021.114584**.

6 J. P. F. Angeli, D. V. Krysko and M. Conrad, Ferroptosis at the crossroads of cancer-acquired drug resistance and immune evasion, *Nat. Rev. Cancer*, 2019, **19**, 405–414, DOI: **10.1038/s41568-019-0149-1**.

7 X. S. Long, X. Hu, S. C. Liu, C. Pan, S. J. Chen, L. H. Li, B. Qi and X. Q. Yang, Insights on preparation, structure and activities of Gracilaria lemaneiformis polysaccharide, *Food Chem.: X*, 2022, **12**, 100153, DOI: **10.1016/j.fochx.2021.100153**.

8 F. L. Shi, X. L. Yan, K. L. Cheong and Y. Liu, Extraction, purification, and characterization of polysaccharides from marine algae Gracilaria lemaneiformis with anti-tumor activity, *Process Biochem.*, 2018, **73**, 197–203, DOI: **10.1016/j.procbio.2018.08.011**.

9 H. Y. Ji, J. Yu, X. D. Dong and A. J. Liu, Preparation of soluble dietary fibers from Gracilaria lemaneiformis and its antitumor activity in vivo, *J. Food Meas. Charact.*, 2019, **13**, 1574–1582, DOI: **10.1007/s11694-019-00073-z**.

10 S. Y. Lu, Y. Liu, S. J. Tang, W. C. Zhang, Q. Y. Yu and C. Q. Shi, *Gracilaria lemaneiformis* polysaccharides alleviate colitis by modulating the gut microbiota and intestinal barrier in mice, *Food Chem.: X*, 2022, **13**, 100197, DOI: 10.1016/j.fochx.2021.100197.

11 X. Du, J. J. Zhang, L. Liu, B. Xu, H. Han, W. J. Dai, X. Y. Pei, X. F. Fu and S. Z. Hou, A novel anticancer property of Lycium barbarum polysaccharide in triggering ferroptosis of breast cancer cells, *J. Zhejiang Univ., Sci., B*, 2022, **23**, 286–299, DOI: 10.1631/jzus.B2100748.

12 H. Q. Shang, X. Y. Niu, W. P. Cui, Z. Sha, C. Wang, T. Huang, P. Guo, X. K. Wang, P. P. Gao, S. Y. Zhang, K. Wei and R. L. Zhu, Anti-tumor activity of polysaccharides extracted from Pinus massoniana pollen in colorectal cancer-in vitro and in vivo studies, *Food Funct.*, 2022, **13**, 6350–6361, DOI: 10.1039/D1FO03908C.

13 T. Di, G. Chen, Y. Sun, S. Ou, X. Zeng and H. Ye, In vitro digestion by saliva, simulated gastric and small intestinal juices and fermentation by human fecal microbiota of sulfated polysaccharides from Gracilaria rubra, *J. Funct. Foods*, 2018, **40**, 18–27, DOI: 10.1016/j.jff.2017.10.040.

14 X. Y. Zhang, S. W. Zhao, X. B. Song, J. W. Jia, Z. Y. Zhang, H. F. Zhou, H. Fu, H. T. Cui, S. Hu, M. J. Fang, X. M. Liu and Y. H. Bian, Inhibition effect of glycyrrhiza polysaccharide (GCP) on tumor growth through regulation of the gut microbiota composition, *J. Pharmacol. Sci.*, 2018, **137**, 324–332, DOI: 10.1016/j.jphs.2018.03.006.

15 T. Afsar, S. Razak, D. Aldisi, M. Shabbir, A. Almajwal, A. A. Al Kheraif and M. Arshad, Acacia hydaspica R. Parker ethyl-acetate extract abrogates cisplatin-induced nephrotoxicity by targeting ROS and inflammatory cytokines, *Sci. Rep.*, 2021, **11**, 17248, DOI: 10.1038/s41598-021-96509-y.

16 Y. Li, J. Liang, Y. Shen, H. X. Kuang and Y. G. Xia, A new application of acetylation for analysis of acidic heteropolysaccharides by liquid chromatography-electrospray mass spectrometry, *Carbohydr. Polym.*, 2020, **245**, 116439, DOI: 10.1016/j.carbpol.2020.116439.

17 S. Veeraperumal, H. M. Qiu, S. S. Zeng, W. Z. Yao, B. P. Wang, Y. Liu and K. L. Cheong, Polysaccharides from Gracilaria lemaneiformis promote the HaCaT keratinocytes wound healing by polarised and directional cell migration, *Carbohydr. Polym.*, 2020, **241**, 116310, DOI: 10.1016/j.carbpol.2020.116310.

18 B. Yang, G. L. Yu, X. Zhao, W. N. Ren, G. L. Jiao, L. H. Fang, Y. H. Wang, G. H. Du, C. Tiller, G. Girouard, C. J. Barrow, H. S. Ewart and J. Z. Zhang, Structural characterisation and bioactivities of hybrid carrageenan-like sulphated galactan from red alga Furcellaria lumbricalis, *Food Chem.*, 2011, **124**, 50–57, DOI: 10.1016/j.foodchem.2010.05.102.

19 T. V. Brito, F. C. N. Barros, R. O. Silva, G. J. Dias, C. J. Simiao, A. X. Franco, P. M. G. Soares, L. S. Chaves, C. M. W. S. Abreu, R. C. M. de Paula, M. H. L. P. Souza, A. L. P. Freitas and A. L. R. Barbosa, Sulfated polysaccharide from the marine algae Hypnea musciformis inhibits TNBS-induced intestinal damage in rats, *Carbohydr. Polym.*, 2016, **151**, 957–964, DOI: 10.1016/j.carbpol.2016.06.047.

20 J. Necas and L. Bartosikova, Carrageenan: a review, *Vet. Med.*, 2013, **58**, 187–205, DOI: 10.17221/6758-VETMED.

21 X. Li, S. M. Huang, X. Chen, Q. J. Xu, Y. X. Ma, L. J. You, V. Kulikouskaya, J. B. Xiao and J. H. Piao, Structural characteristic of a sulfated polysaccharide from Gracilaria Lemaneiformis and its lipid metabolism regulation effect, *Food Funct.*, 2020, **11**, 10876, DOI: 10.1039/D0FO02575E.

22 F. C. N. Barros, D. C. da Silva, V. G. Sombra, J. S. Maciel, J. P. A. Feitosa, A. L. P. Freitas and R. C. M. de Paula, Structural characterization of polysaccharide obtained from red seaweed Gracilaria caudata (J Agardh), *Carbohydr. Polym.*, 2013, **92**, 598–603, DOI: 10.1016/j.carbpol.2012.09.009.

23 P. Salehi, Y. Dashti, F. M. Tajabadi, F. Safidkon and R. Rabei, Structural and compositional characteristic of a sulfated galactan from the red alga Gracilariopsis persica, *Carbohydr. Polym.*, 2011, **83**, 1570–1574, DOI: 10.1016/j.carbpol.2010.10.017.

24 A. O. Kravchenko, A. O. B. Barabanova, V. P. Glazunov, I. M. Yakovleva and I. M. Yermak, Seasonal variations in a polysaccharide composition of Far Eastern red seaweed Ahnfeltiopsis flabelliformis (Phyllophoraceae), *J. Appl. Phycol.*, 2018, **30**, 535–545, DOI: 10.1007/s10811-017-1262-8.

25 V. C. G. Schnoller, G. Hernandez-Carmona, E. Hernandez-Garibay, J. M. Lopez-Vivae and M. Munoz-Ochoa, Chemical characterization of soluble polysaccharides in the red alga *Acanthophora spicifera* from La Paz Bay, Baja California Sur, Mexico, *Cienc. Mar.*, 2020, **46**, 165–176, DOI: 10.7773/cm.v46i3.3090.

26 J. L. Roh, E. H. Kim, H. J. Jang, J. Y. Park and D. Shin, Induction of ferroptotic cell death for overcoming cisplatin resistance of head and neck cancer, *Cancer Lett.*, 2016, **381**, 96–103, DOI: 10.1016/j.canlet.2016.07.035.

27 L. M. Xie, M. Y. Shen, Y. Z. Hong, H. D. Ye, L. X. Huang and J. H. Xie, Chemical modifications of polysaccharides and their anti-tumor activities, *Carbohydr. Polym.*, 2019, **229**, 115436, DOI: 10.1016/j.carbpol.2019.115436.

28 F. G. Zhai, Q. C. Liang, Y. Y. Wu, J. Q. Liu and J. W. Liu, Red ginseng polysaccharide exhibits anticancer activity through GPX4 downregulation-induced ferroptosis, *Pharm. Biol.*, 2022, **60**, 909–914, DOI: 10.1080/13880209.2022.2066139.

29 Y. Kang, Z. J. Wang, D. S. Xie, W. G. Yang, X. D. Zhao and N. J. Xu, Characterization and potential antitumor activity of polysaccharide from Gracilariopsis lemaneiformis, *Mar. Drugs*, 2017, **15**, 100, DOI: 10.3390/md15040100.

30 S. M. T. Gharibzahedi, F. J. Marti-Quijal, F. J. Barba and Z. Altinas, Current emerging trends in antitumor activities of polysaccharides extracted by microwave- and ultrasound-assisted methods, *Int. J. Biol. Macromol.*, 2022, **202**, 494–507, DOI: 10.1016/j.ijbiomac.2022.01.088.

31 J. Kang, X. Jia, N. F. Wang, M. Xiao, S. Song, S. Wu, S. W. Cui and Q. B. Guo, Insights into the structure-bioactivity relationships of marine sulfated polysaccharides: a review, *Food Hydrocolloids*, 2022, **123**, 107049, DOI: 10.1016/j.foodhyd.2021.107049.

32 Y. Y. Sun, C. X. Zhang, P. P. Zhang, C. Q. Ai and S. Song, Digestion characteristic of polysaccharides from Gracilaria

lemaneiformis and its interaction with the human gut microbiota, *Int. J. Biol. Macromol.*, 2022, **213**, 305–316, DOI: **10.1016/j.ijbiomac.2022.05.172**.

33 Y. L. Fan, W. H. Wang, W. Song, H. S. Chen, A. G. Teng and A. J. Liu, Partial characterization and anti-tumor activity of an acidic polysaccharide from Gracilaria lemaneiformis, *Carbohydr. Polym.*, 2012, **88**, 1313–1318, DOI: **10.1016/j.carbpol.2012.02.014**.

34 M. J. Munro, S. K. Wichremesekera, S. T. Tan and L. F. Peng, Proteomic analysis of low- and high-grade human colon adenocarcinoma tissues and tissue-derived primary cell lines reveals unique biological functions of tumours and new protein biomarker candidates, *Clin. Proteomics*, 2022, **10**, 27, DOI: **10.1186/s12014-022-09364-y**.

35 J. Song, T. T. Liu, Y. Yin, W. Zhao, Z. Q. Lin, Y. X. Yin, D. Lu and F. P. You, The deubiquitinase OTUD1 enhances iron transport and potentiates host antitumor immunity, *EMBO Rep.*, 2021, **22**, e51162, DOI: **10.15252/embr.202051162**.

36 S. Rockfield, R. Chhabra, M. Robertson, N. Rehman, R. Bisht and M. Nanjundan, Links between iron and lipids: implications in some major human diseases, *Pharmaceuticals*, 2019, **11**, 113, DOI: **10.3390/ph11040113**.

37 Z. J. Wang, X. N. Chen and Z. Jiang, Immune infiltration and a ferroptosis-related gene signature for predicting the prognosis of patients with cholangiocarcinoma, *Am. J. Transl. Res.*, 2022, **14**, 1204–1219 **https://www.ncbi.nlm.nih.gov/pmc/articles/PMC8902578/**.

38 L. Zhao, X. X. Zhou, F. Xie, L. Zhang, H. Y. Yan, J. Huang, C. Zhang, F. F. Zhou, J. Chen and L. Zhang, Ferroptosis in cancer and cancer immunotherapy, *Cancer Commun.*, 2022, **42**, 88–116, DOI: **10.1002/cac2.12250**.

39 Y. H. Wang, Z. Y. Zhang, W. C. Sun, J. Zhang, Q. Y. Xu, X. R. Zhou and L. M. Mao, Ferroptosis in colorectal cancer: potential mechanisms and effective therapeutic targets, *Biomed. Pharmacother.*, 2022, **153**, 113524, DOI: **10.1016/j.biopha.2022.113524**.

40 F. J. Li, H. Z. Long, Z. W. Zhou, H. Y. Luo, S. G. Xu and L. C. Gao, System Xc-/GSH/GPX4 axis: an important antioxidant system for the ferroptosis in drug-resistant solid tumor therapy, *Front. Pharmacol.*, 2022, **13**, 910292, DOI: **10.3389/fphar.2022.910292**.

41 B. F. Tang, J. Y. Zhu, J. Li, J. Li, K. Fan, Y. Gao, S. M. Cheng, C. L. Kong, L. Y. Zheng, F. Z. Wu, Q. Y. Weng, C. Y. Lu and J. S. Ji, The ferroptosis and iron-metabolism signature robustly predicts clinical diagnosis, prognosis and immune microenvironment for hepatocellular carcinoma, *Cell Commun. Signaling*, 2020, **18**, 174, DOI: **10.1186/s12964-020-00663-1**.

42 X. T. Xu, X. Y. Zhang, C. Q. Wei, D. X. Zheng, X. Lu, Y. Y. Yang, A. L. Luo, K. F. Zhang, X. Q. Duan and Y. H. Wang, Targeting SLC7A11 specifically suppresses the progression of colorectal cancer stem cells via inducing ferroptosis, *Eur. J. Pharm. Sci.*, 2020, **152**, 105450, DOI: **10.1016/j.ejps.2020.105450**.

43 K. Shan, N. H. Feng, D. D. Zhu, H. Y. Qu, G. L. Fu, J. Q. Li, J. Cui, H. Y. Chen, R. Wang, Y. M. Qi and Y. Q. Chen, Free docosahexaenoic acid promotes ferroptotic cell death via lipoxygenase dependent and independent pathways in cancer cells, *Eur. J. Nutr.*, 2022, **61**, 4059–4075, DOI: **10.1007/s00394-022-02940-w**.

44 M. A. Badgley, D. M. Kremer, H. C. Maurer, K. E. Delgiorno, H. J. Lee, V. Purohit, I. R. Sagalovskiy, A. Ma, J. Kapilian, C. E. M. Decker, S. A. Sastra, C. F. Palermo, L. R. Andrade, P. Sajjakulnukit, L. Zhang, Z. P. Tolstyka, T. Hirschhorn, C. lamb, T. Liu, W. Gu, E. S. Seeley, E. Stone, G. Georgiou, U. Manor, A. Iuga, G. M. Wahl, B. R. Stockwell, C. A. Lyssiotis and K. P. Olive, Cysteine depletion induces pancreatic tumor ferroptosis in mice, *Science*, 2020, **368**, 85–89, DOI: **10.1126/science.aaw9872**.

45 C. X. Xu, S. G. Sun, T. Johnso, R. Qi, S. Y. Zhang, S. Y. Zhang and K. Yang, The glutathione peroxidase Gpx4 prevents lipid peroxidation and ferroptosis to sustain Treg cell activation and suppression of antitumor immunity, *Cell Rep.*, 2021, **35**, 109235, DOI: **10.1016/j.celrep.2021.109235**.

46 J. R. Ren, Y. Z. Lv, L. L. Wu, S. L. Chen, C. X. Lei, D. Yang, F. D. Li, C. Z. Liu and Y. H. Zheng, Key ferroptosis-related genes in abdominal aortic aneurysm formation and rupture as determined by combining bioinformatics techniques, *Front. Cardiovasc. Med.*, 2022, **9**, 875434, DOI: **10.3389/fcvm.2022.875434**.